Journal of Sound and Vibration 329 (2010) 2306–2322

Contents lists available at ScienceDirect

Journal of Sound and Vibration

journal homepage: www.elsevier.com/locate/jsvi

Guided wave health monitoring of complex structures by sparse array systems: Influence of temperature changes on performance

T. Clarke, F. Simonetti, P. Cawley *

Research Centre in Non-Destructive Evaluation, Imperial College London, UK

ARTICLE INFO

Article history:
Accepted 28 January 2009
The peer review of this article was organised by the Guest Editor
Available online 4 March 2009

ABSTRACT

Structural health monitoring of complex structures with guided waves is complicated because of the large number of overlapping reflections obtained in time-traces. One of the strategies to avoid having to interpret raw time signals is to use baseline subtraction techniques. However, environmental effects modify the signals, causing large amplitude levels in the subtracted signal which can mask information received from weak reflectors such as defects. A large database of baselines covering environmental effects commonly faced by the structure becomes necessary, and the simple gathering of these baselines becomes a difficult task. This paper investigates how a temperature compensation method can be used to reduce the number of signals required in the database. The strong influence of signal complexity and mode purity on the effectiveness of this method is shown experimentally. Finally, an airframe panel is tested using a temperature compensation strategy developed.

1. Introduction

Structural health monitoring of complex structures is an increasingly important topic particularly for aerospace applications, but also in the oil and gas, nuclear and shipping industries. Techniques based on sparse arrays of sensors which generate and receive guided waves are among the most promising candidates [1–7]. Guided waves propagate over large distances and certain modes have the ability to transmit through a variety of structural features leading to a relatively small number of sensors being able to cover the structure.

In structures containing high densities of structural elements, the time-traces obtained are often too complex to be directly interpreted due to the large number of overlapping reflections. In this case, the baseline subtraction technique becomes attractive [8,9]. In this method a current signal from the structure is subtracted from a signal which has been acquired during the initial stages of operation of the structure. This eliminates the need for interpretation of the complex raw time signal and any defects will be clearly seen provided the amplitude of the residual signal obtained after subtraction of the baseline signal is sufficiently low when the structure is undamaged. The ideal amplitude level of the residual signal should be close to −40 dB relative to the amplitude of the first arrival in a pitch-catch configuration since reflections from defects are likely to produce levels of −30 dB or lower [10–13].

Temperature has a great influence on transducer performance and on wave propagation [14,15]. Influence on transduction can be eliminated by careful material selection and packaging techniques. Wave propagation is affected when the elastic properties and density of the propagating medium are shifted. This means significant changes in signals will

* Corresponding author. Tel.: +44 207 594 7227; fax: +44 207 584 1560.
E-mail address: p.cawley@imperial.ac.uk (P. Cawley).

0022-460X/$ - see front matter © 2009 Elsevier Ltd. All rights reserved.
doi:10.1016/j.jsv.2009.01.052

happen even with very small ($<0.5\,^{\circ}$C) temperature drifts. Testing of the structure will happen over a range of temperatures which are bound to change significantly the signals obtained. Approaches to overcome this problem are presented in Refs. [15,16], and are called baseline selection or optimal baseline subtraction; these involve the use of a database of signals that represents environmental conditions commonly faced by the undamaged structure which are recorded during the initial stages of operation. The current signal is compared to each signal in the database and the optimal baseline signal will be the one which gives the lowest residual. However, to reach the targeted levels of amplitude in the residual signal, the temperature interval needed between baselines is very small. As will be demonstrated, an impractical number of baselines would be necessary to ensure acceptable results if only baseline subtraction is used.

Temperature compensation techniques [9,17] can be used in conjunction with optimal baseline subtraction to increase the allowable temperature gap between baseline signals and therefore to reduce the number of signals in the database. However, these techniques may be affected by the complexity of the signals and the degree of mode purity.

This paper begins by discussing the influence of mode purity and signal complexity on signal processing techniques for temperature compensation. Experimental setups consisting of simple pitch-catch arrangements using transducers generating different *A*0/*S*0 mode ratios at a range of frequencies were used. The spatial frequency of reflectors was also varied by testing plates of different sizes. The effects are quantified so the minimum number of baselines necessary for a robust SHM system is identified. Finally, a real complex structure is monitored using the signal processing strategy described.

2. Influence of temperature on wave propagation and baseline subtraction

The influence of temperature on wave propagation was demonstrated in Ref. [16]. Two Hanning-windowed tone bursts are considered, I_0 and I_1, which represent the baseline and the current signal, respectively. The current signal is taken at a different temperature so it is expanded in time by δt, which is the time shift:

$$I_0 = u_0 h(t) \sin \omega t \tag{1}$$

$$I_1 = u_0 h(t) \sin \omega(t+\delta t) \tag{2}$$

where $h(t)$ is the Hanning window function, u_0 is the amplitude, ω, the angular frequency, and t is time. As demonstrated in Ref. [16], the time shift for direct subtraction can be represented as

$$\delta t = \frac{d}{v}(\alpha-\gamma)\delta T \tag{3}$$

where γ is the fractional change in phase velocity with temperature, k/v, k being the coefficient of change in phase velocity with temperature and v the phase velocity; δT is the variation in temperature, d is the propagation distance, and α is the coefficient of thermal expansion. Eq. (3) shows that change in wave velocity due to temperature drifts is the main cause of time shift in signals, since γ is typically significantly larger than α. It also shows that increases in temperature will always cause a positive δt, as this will increase the propagation path due to thermal expansion of the structure and reduce phase velocity values, since, as mentioned in [16], a typical value of k is $-1\,\mathrm{m\,s^{-1}\,^{\circ}C^{-1}}$. Eq. (3) can be simplified to

$$\delta t = \frac{d}{v}\beta\delta T \tag{4}$$

where β is $(\alpha-\gamma)$. If the concept of baseline subtraction is applied, I_1 is subtracted from $I_{0,}$ and defining $U_0 = u_0 h(t)$

$$I_1 - I_0 = U_0(\sin\omega(t+\delta t) - \sin\omega t) \tag{5}$$

By assuming that δt is small enough to allow a small angle approximation:

$$|I_1 - I_0|_{\max} = 2\pi f U_0 \delta t \tag{6}$$

where f is frequency.

It follows from the development of Eq. (5) that if two waves of equal amplitude arrive in phase, the amplitude of the residual signal will be doubled. When the number of reflectors increases, as in a complex structure, interference will happen more frequently, so the maximum residue after baseline subtraction will increase. This suggests that the residual signal is proportional to the temperature difference between the current signal and baseline (expressed by the time shift), to the number of overlapping arrivals and to the excitation frequency.

However, by combining Eqs. (4) and (6) and considering $\lambda = v/f$

$$|I_1 - I_0|_{\max} = 2\pi\frac{d}{\lambda}U_0\beta\delta T \tag{7}$$

Eq. (7) shows that the residual level is proportional to the propagation distance expressed in wavelengths rather than simply to the frequency; only if the velocity is constant with frequency (i.e. the mode is non-dispersive) is the residual for a given propagation distance simply proportional to frequency. This is an important issue when selecting the mode and frequency which will be used by the monitoring system.

3. Specimens and test setup

Fig. 1 shows a sketch of the simple pitch-catch system used in this work. Two steel plates of 5 mm thickness and lengths L of 1 and 0.4 m were used. All other dimensions, including positioning of the transducers, were kept proportional to L. The system was placed in a temperature controlled environment where the temperature was gradually increased by 10 °C over 3 h and then cooled back to ambient temperature over 2 h, signals being acquired at 0.1 °C steps. This cycle was repeated with an interval of a day and signals obtained during the first cycle were used as baselines while signals from the second cycle were considered current signals. Therefore, for each value of temperature within the 10 °C range considered, two signals, recorded during heating and cooling of the system, were present in the database. The temperature was monitored by type-K thermocouples soldered to the plate next to the transducers. Temperature was read to a precision of 0.1 °C.

Two types of piezoelectric transducers were used: one generating an almost pure $A0$ mode at low frequencies, and the other generating different $S0/A0$ ratios at two higher frequencies. Both transducers were attached to the plates with epoxy adhesive (Loctite Hysol E-05CL) which was room temperature cured for 36 h and cycled at temperatures above those expected during operation to avoid post-curing effects and to relieve residual stresses in the bond layer which lead to changes in stiffness during operation [18]. Constant pressure was applied to the transducer during curing so that a thin bond line was obtained; this reduces the influence of change in the bond line on transducer behaviour.

The low-frequency $A0$ transducer uses a backing mass and a soft front layer to lower the through-thickness resonance frequency of a piezoelectric element to around 20 kHz for a 3 mm thick front layer. The presence of the front layer allows the system to be modelled as a simple spring-mass system as shown in Fig. 2a where a sketch of the system can also be seen. The front layer, in this case made of silicon carbide (SiC) foam, also reduces transmission of unwanted in-plane motion, caused by Poisson's ratio effects in the piezoelectric element, which would lead to excitation of the $S0$ mode in the structure.

The ratio of the amplitudes of the $A0$ and $S0$ modes was obtained by finite element modelling of the transducers attached to a 5 mm-thick, 1 m-long steel plate, in pulse-echo mode, with the piezoelectric behaviour of the transducer included in the model. Excitation was achieved by applying a voltage signal to the top surface of the piezoelectric element while the bottom surface was grounded, simulating the experimental setup. Bond layers were included in the finite element models as a line of quadratic elements of the same dimension as in the rest of the model (0.25 mm square), with material properties of epoxy (Young's modulus: 2.8 GPa; density: 1200 Kg m^{-3}; Poisson's ratio: 0.345). It was found that small changes in bond line thickness did not significantly influence the predictions; this was thought to be because of the similarity between the elastic properties of epoxy and SiC foam which meant that a change in bond line thickness had a similar effect to a small change in the thickness of the interlayer. Damping was also included in the bond layers; for this, values of $G_l/G_\infty = 0.3$ and $E_l/E_\infty = 0.3$ were used, where G and E are the shear and Young's moduli, respectively, and the subscripts l and ∞ stand for the loss modulus and the long-term modulus, respectively (for further details on the damping parameters used, see Ref. [19]). The transducer generated a wave in the plate which was reflected at the edge and propagated back to the transducer. Due to the significant differences in velocity between the two modes and the large propagation distance involved, the reflection of the two modes could be separated in time and when these signals were received by the transducer a voltage time trace was generated; this was used to obtain the mode amplitude ratios. To avoid dispersion effects which cause reduction of amplitude due to spread of the signals in time, the computation of the ratio was carried out in the frequency domain. The mode ratio obtained from this procedure is that obtained in signals when using a given transducer type in pulse-echo or pitch-catch mode. When the low-frequency $A0$ transducer was modelled with

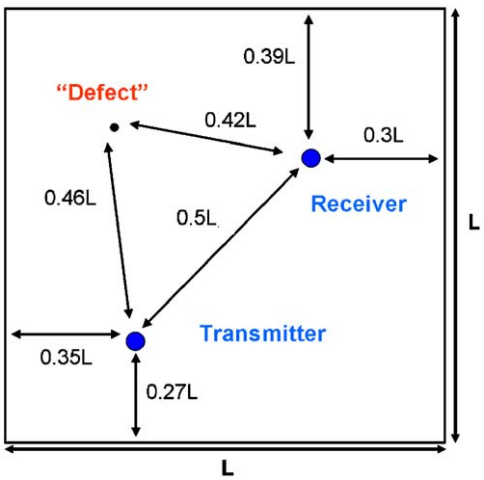

Fig. 1. Schematic diagram of positioning of transducers and defect as a function of plate length L.

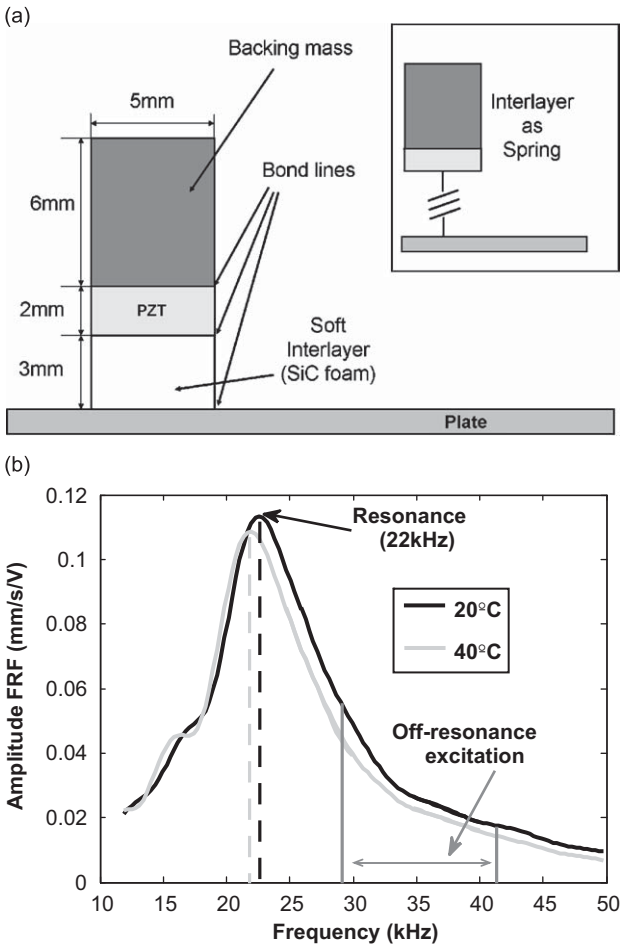

Fig. 2. (a) Schematic diagram of low-frequency pure *A*0 transducer; (b) frequency-response function of the same transducer with a 20 °C temperature shift.

dimensions as shown in Fig. 2a, the received voltage time trace obtained showed a ratio between the *A*0 and *S*0 mode signals of 73 dB. When a transducer with the same geometry but with no interlayer was modelled under the same conditions, an *A*0/*S*0 mode voltage ratio of 38 dB was obtained at the new resonance of the system (100 kHz).

To evaluate the temperature stability of the *A*0 transducer on a 5 mm-thick aluminium plate, the frequency-response function (FRF) of the transducer was obtained by focusing a laser interferometer, measuring out-of-plane velocity, on the backing mass of the transducer and dividing the frequency content of the measured signal by the frequency content of the input signal. Fig. 2b shows the FRF obtained using this procedure at 20 °C, the resonance of the system being at 22 kHz. Fig. 2b also shows the FRF obtained for the system at 40 °C; an expected significant change in the FRF is seen in the vicinity of the resonance suggesting the occurrence of phase shifts. Phase stability is a key requirement of the transducer if baseline subtraction is to be used, so it is necessary to operate off resonance. It was found that operation at 35 kHz centre frequency caused minor amplitude variations to occur, which can be easily corrected for, phase shifts being negligible. Excitation of the transducer in this frequency region also produced adequate signal amplitude in the structure, therefore giving a good compromise between stability and transmitted energy. Details of the design, behaviour and temperature stability of this transducer can be found in Ref. [20].

The other transducer used in the experiments was a 20 mm diameter, 1 mm thick piezoelectric disc, as used in Ref. [17]. The frequency response of the waves generated in the plate by this piezoelectric element shows a sharp drop in excitation of the *A*0 mode at around 150 kHz when the ratio of the diameter of the disc to the wavelength of this mode approaches unity. Therefore, when excited with a five-cycle Hanning windowed toneburst with a centre frequency of 150 kHz, a 17 dB *S*0/*A*0 mode received voltage ratio is obtained in a pulse-echo configuration. If the element is excited with a similar signal centred at 200 kHz, which is above the sharp drop in excitation of the *A*0 mode, the *S*0/*A*0 mode ratio is reduced to 8 dB. The *S*0 mode excitation is relatively constant in the 100–300 kHz frequency range. This leads to adequate temperature stability over the entire excitation frequency range; the phase stability is good, only amplitude changes being found, which can be easily compensated for.

To validate the FE models, the out-of-plane displacement monitored on the surface of the plate generated by each transducer in the model was compared to signals obtained when an identical experimental setup was used, with a laser vibrometer measuring out-of-plane displacement at the surface of the plate. Good agreement between experimental and FE results was found in all cases. In the *A*0 mode transducer case, errors between the FE- and experimentally obtained FRF were within 10 percent for amplitude and frequency content and within 5 percent for the *A*0/*S*0 mode amplitude ratio; in the *S*0 mode transducer case the amplitude ratio between the two modes matched the FE-obtained voltage ratio within an error of 5 percent.

A PC was used to upload input signals to an arbitrary function generator (Agilent 33220) which was connected through an amplifier to the emitting transducer. The signal from the receiver was pre-amplified and acquired via a 12-bit PC-based oscilloscope set to 100 averages.

A brass cylinder of 5 mm diameter and 6 mm length was attached to the surface of the plates with a couplant to simulate a weak reflector or "defect". The position of this simulated defect is indicated in Fig. 1.

4. Temperature compensation methods

4.1. Optimal baseline method

The optimal baseline method is based on the identification of a signal within a database which is most similar to a current signal taken from the structure during inspection. If the two signals are similar enough, low levels of residual will be achieved when the two are subtracted in the absence of a defect. Since environmental effects are the main reason for changes in the response of the system, the optimal baseline method is effectively a search for the signal which has been taken at environmental conditions similar to those found during inspection. The database of signals will have been previously acquired during the initial stages of operation of the structure after conventional NDE techniques have been used to search for manufacturing defects.

The selection of the optimal baseline is generally done by subtracting all the signals in a database from the signal currently taken during inspection. The choice of best baseline is done by monitoring a value which describes the amplitude of the residual signal. It is clear that a large database, covering all environmental conditions likely to seen in practice, is necessary if small residual levels are to be obtained with this method.

As demonstrated in Ref. [15], the minimum level of residual in not necessarily found when the current signal is subtracted from a baseline taken at exactly the same temperature at an earlier stage; the optimal baseline is often a signal taken at a slightly different temperature, the difference typically being of the order of 0.1 °C. This effect may be attributable to uncertainties in temperature measurement.

4.2. Optimal stretch method

As seen in Section 2, temperature changes affect the velocities of the different modes besides causing expansion or contraction of the structure. These changes cause signals to arrive earlier or later in time; this effect is cumulative so that later parts of the signal, corresponding to larger propagation distances, suffer larger absolute delays.

Several related methods for correcting this effect have been presented in the literature based on time domain stretching [21] of either the reference signal or the current signal, estimation of delay as a function of time through local coherence and use of these values as factors for subsequent time-domain stretch [9,14], or simple frequency domain stretch [17,20]. Stretching of the signal in time or frequency causes dilations of wave-packets as well as arrival times; this means that these techniques do not compensate perfectly for temperature effects since the frequency content of the signal is altered.

In this paper the correction was made in the frequency domain by stretching the frequency axis. Fig. 3a shows part of the spectrum of a reference signal and of a second signal taken with a temperature difference of 10 °C. To compensate for the small difference between the two spectra, the frequency step size, Δf, of the spectrum of the second signal was stretched or compressed in small steps. In each step, the stretched spectrum of the second signal would be multiplied by the ratio between the spectrum of the input signal and the stretched spectrum of the input signal; this is a correction factor for spectrum distortion effects, as described in Ref. [17]. The optimal stretch corresponds to the minimum of the residual signal in time or to the maximum in correlation between the spectra of the two signals. Fig. 3b shows the best match between the spectra of the two signals shown in Fig. 3a. Small differences in the overall amplitude of the two spectra are compensated by normalising the power content of each signal in the frequency domain. This amplitude correction in the frequency domain occasionally leads to excessive or insufficient amplitude corrections at certain frequencies, as can be seen, for example, in the region around 26 kHz in Fig. 3b, but the overall amplitude differences in the time domain are considerably improved.

4.3. Filtering of noise in the subtracted signal

When the optimal stretch method is used to compensate for a temperature gap between a reference and a current signal, differences in matching of different regions of the spectrum are often seen. This unequal matching occurs because

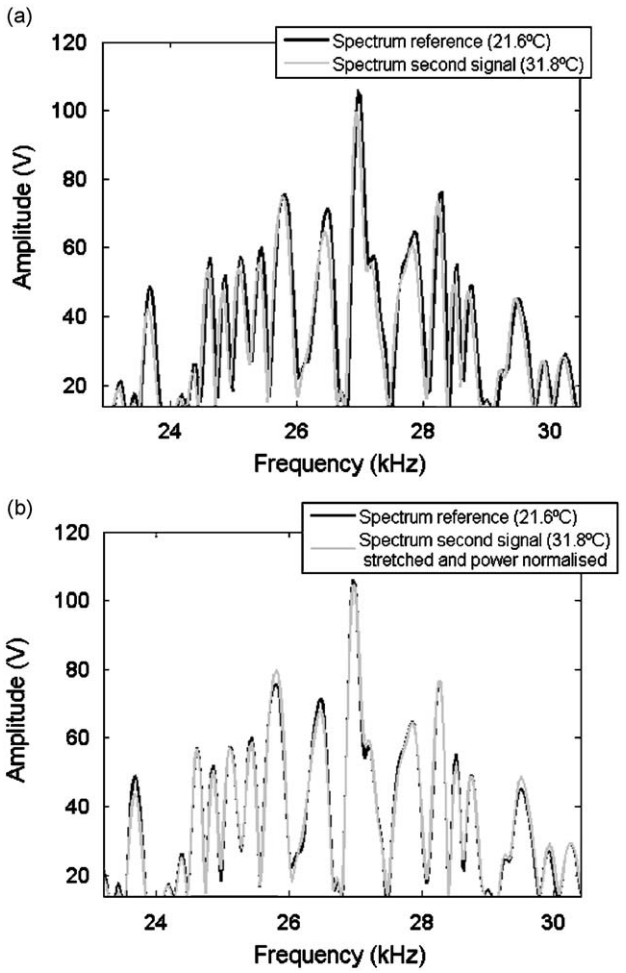

Fig. 3. (a) Spectrum of the reference signal (21.8 °C) and of the current signal (31.8 °C); (b) spectrum of the reference signal (21.8 °C) and of the current signal (31.8 °C) after optimal stretch and power normalisation.

the centre frequency of the spectrum of the two signals is where the largest power is concentrated and, therefore, the highest amplitude is found. Consequently, the best match of the region close to the centre frequency during stretch of the frequency axis will cause the sharpest drop in the rms of the residual signal. However, the quality of the match in other parts of spectrum is less good and analysis of the frequency content of the subtracted signal shows that high levels of residue are found at frequencies above or below the centre frequency region. Fig. 4 shows the spectrum of the residual of the subtracted signal between a reference and a current signal with a 10 °C temperature difference. High amplitudes are seen at frequencies below the centre frequency of the input signal (35 kHz). A filter with bandwidth equivalent to that of a seven-cycle Hanning windowed toneburst was used to eliminate the unwanted regions of the spectrum of the subtracted signal. The use of such a simple bandpass filter can give a 5–10 dB reduction of amplitude levels in the residual. The bandwidth of the filter was chosen as a compromise between reduction of noise levels and maintenance of sufficient spatial resolution for defect localisation. Further description of this method and of the type of noise found in the spectrum of the subtracted signal can be found in Ref. [20].

5. Results for different plate sizes

Results presented in this section were obtained by using two low-frequency *A*0 transducers in a pitch-catch configuration on the two plate sizes, with dimensions as described in Section 3 and Fig. 1.

5.1. Optimal baseline method

Fig. 5a shows the signal obtained from the large plate at a temperature of 28.9 °C and the residue obtained when this signal and the selected optimal baseline, which was taken on the previous day at 29.0 °C, are subtracted. The first arrival

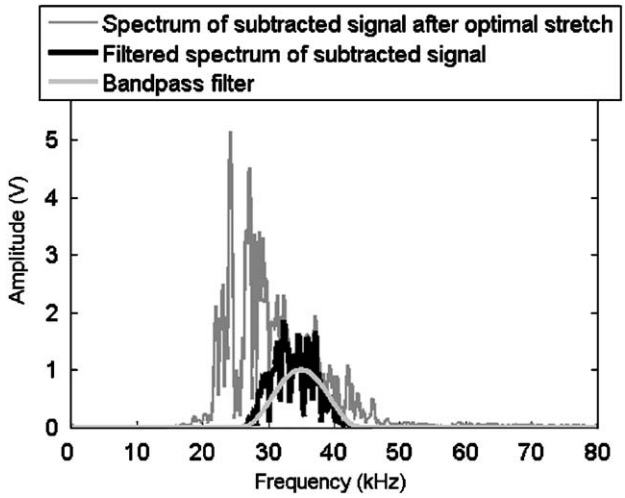

Fig. 4. Spectrum of the signal obtained from subtraction between a reference signal and a current signal with 10 °C temperature difference after optimal stretch processing, the bandpass filter used to eliminate noise and the filtered spectrum.

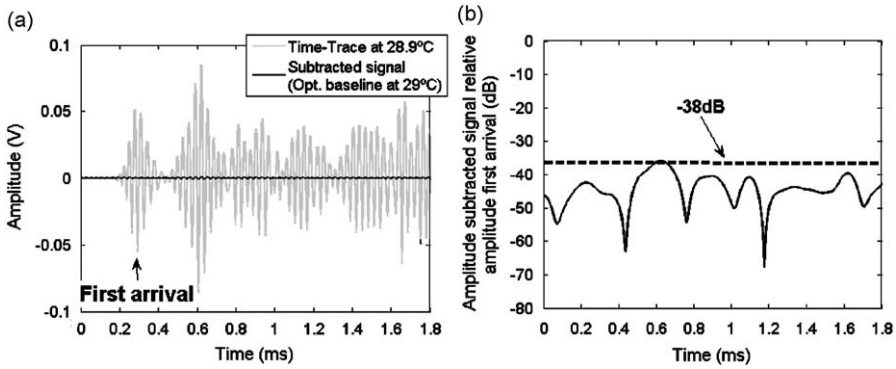

Fig. 5. (a) Signal taken at 28.9 °C and the signal obtained when subtracted from baseline (29 °C) on the large plate; (b) amplitude of the subtracted signal relative to amplitude of the first arrival in Fig. 5a.

can clearly be seen and multiple reflections from the edges of the plate arrive later. The noise levels in the subtracted signal relative to the amplitude of the first arrival are shown in Fig. 5b and correspond to a worst case of −38 dB. This value is close to the target of −40 dB but these results demonstrate how small the temperature gaps between baselines need to be to ensure satisfactory results. It was noted that the direction of the temperature variation of the structure within the cycle did not influence the behaviour of the algorithm; the optimal baseline selected by the algorithm for a signal taken during cooling of the structure in the second cycle, for example, was equally likely to be selected from the heating or cooling stages of the first cycle.

Fig. 6a shows the signal obtained for the small plate at 32.6 °C and the residual signal after subtraction from the optimal baseline, which in this case was taken at 32.5 °C. The decay rate of the signal in Fig. 6a is much higher than that of the corresponding signal on the large plate (Fig. 5a). This is thought to be due to mode conversion at the edges, which are not perfectly normal to the surface, and to attenuation and mode conversion at transducer bond lines. In the small plate there are more interactions with the edges and bond lines in a given time than on the large plate (propagation equivalent to one side length takes 0.18 ms in the small plate and 0.45 ms in the large plate).

Fig. 6b shows that the level of residue obtained, −39 dB relative to the first arrival in Fig. 6a, is also close to the target of −40 dB. In the simpler signal of Fig. 2, only one time region was responsible for the worst residual amplitude value, which was the point (0.6 ms) where four reflections from the edges overlap. The corresponding point in the small plate is at 0.25 ms, but since the distances between reflectors are smaller than in the large plate case, strong overlapping of reflections happens throughout the entire signal.

Figs. 7a and b show the residual levels after subtraction of signals taken on the large plate and the small plate with a temperature gap of 0.3 °C. This simulates the effect of the baseline data set being obtained with a larger temperature step size. In both cases the worst residual level is increased to around −31 dB relative to the first arrival. This shows that if the

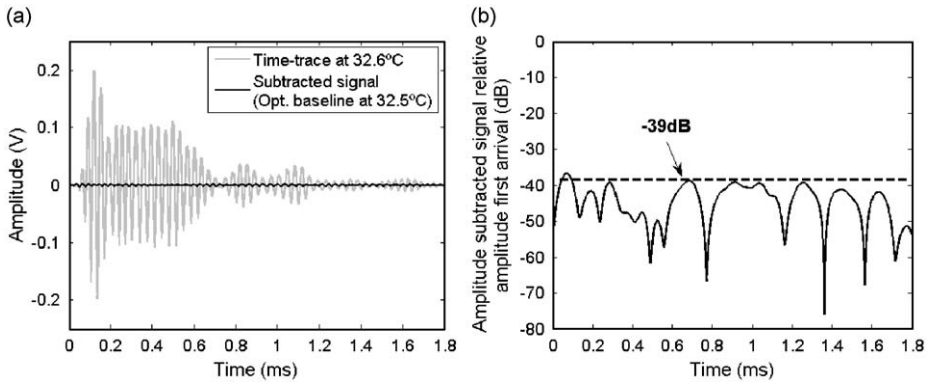

Fig. 6. (a) Signal taken at 32.6 °C and the signal obtained when subtracted from baseline (32.4 °C) on the small plate; (b) amplitude of the subtracted signal relative to amplitude of the first arrival in Fig. 6a.

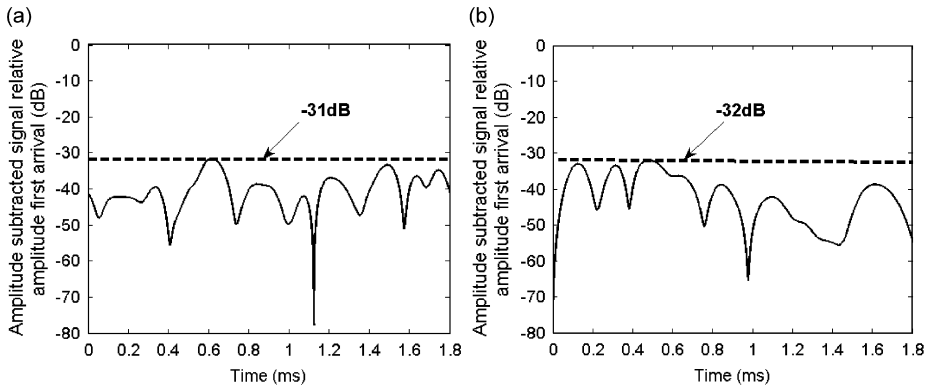

Fig. 7. Residual levels after subtraction for (a) large plate and (b) small plate with a temperature gap between current signal and baseline of 0.3 °C (current signal at 32.6 °C, baseline at 32.3 °C), relative to the first arrival.

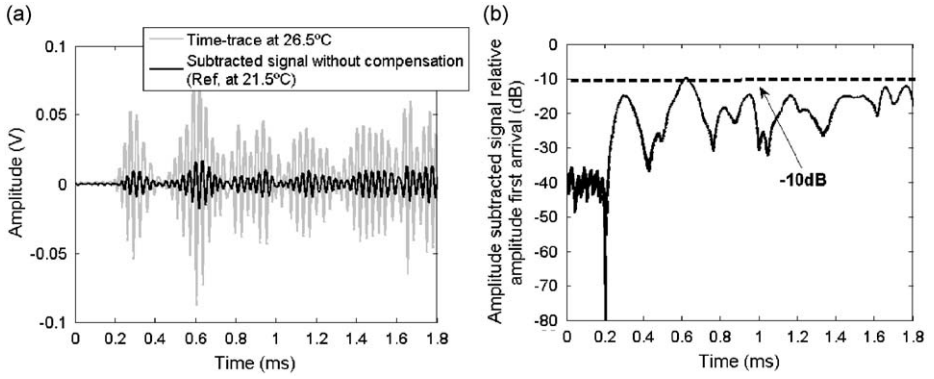

Fig. 8. (a) Signal taken at 26.5 °C and the signal obtained from immediate subtraction from baseline (21.5 °C) on the large plate; (b) amplitude of the subtracted signal relative to amplitude of the first arrival in Fig. 8a.

optimal baseline method is used alone it is necessary to store a very large baseline set at small temperature step sizes (0.1 °C), which is likely to be impractical to store and difficult to obtain.

5.2. Optimal stretch method

For the results shown in this section, a signal taken at room temperature (21.5 °C) will be taken as the reference and the effectiveness of the optimal stretch method will be evaluated for a current signal taken 5 °C above reference. This temperature difference was considered a challenging test for the robustness of the optimal stretch method because high

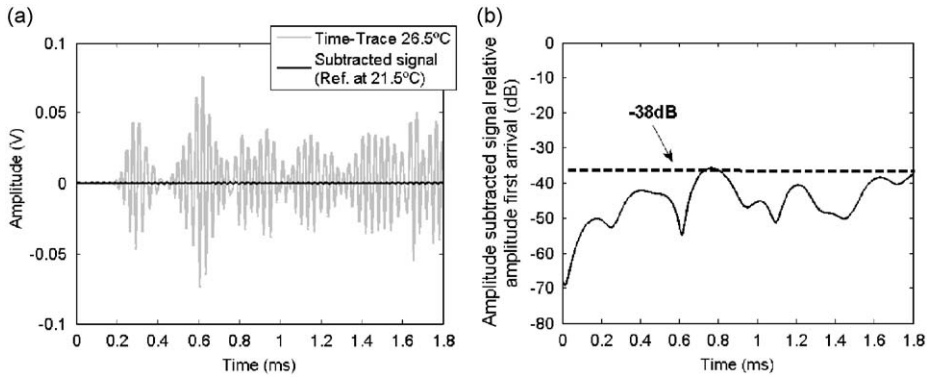

Fig. 9. (a) Signal taken at 26.5 °C and the signal obtained when subtracted from stretched reference (21.5 °C) on the large plate; (b) amplitude of the subtracted signal relative to amplitude of the first arrival in Fig. 9a.

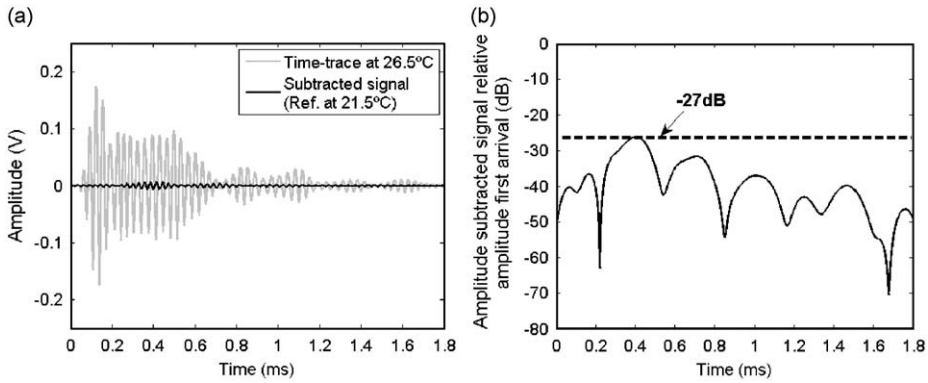

Fig. 10. (a) Signal taken at 26.5 °C and the signal obtained when subtracted from stretched reference (21.5 °C) on the small plate; (b) amplitude of the subtracted signal relative to amplitude of the first arrival in Fig. 10a.

levels of residual are found for direct subtraction of the two signals as seen in Fig. 8a, which shows the signal taken from the large plate at 26.5 °C and the signal obtained after direct subtraction from the baseline at 21.5 °C. Fig. 8b shows that the worst amplitude level in the residual reaches −10 dB relative to the first arrival.

Fig. 9a shows the signal obtained after temperature compensation of the signal of Fig. 8 through the optimal stretch method. The amplitude levels in the subtracted signal are around −38 dB relative to the first arrival seen in Fig. 9a for a 5 °C temperature change, as can be seen in Fig. 9b. This is a large improvement compared to the value of the signal obtained from direct subtraction (−10 dB relative to the first arrival, as shown in Fig. 8).

The same procedure was repeated for signals obtained on the small plate. The worst amplitude level in the residual signal after direct subtraction between a signal taken at 26.5 °C and a baseline at 21.5 °C was −11 dB relative to the first arrival. This level is similar to the result obtained for direct subtraction between two signals taken at the same temperatures on the large plate (as was seen in Fig. 8).

When the optimal stretch technique is used to compensate for the 5 °C temperature difference between the signals taken from the small plate, the residual signal level shown in Fig. 10 is obtained after subtraction. A worst value of −27 dB relative to the first arrival was found; this is far from the target value of −40 dB and much poorer than the performance of the method on the signals taken on the large plate. This difference between the large and small plates was seen consistently in data from multiple experiments. This suggests that the effectiveness of the optimal stretch method in compensating for large temperature differences is reduced when it is applied to more complex signals comprising a large number of reflections. The optimal stretch method therefore has limited applicability on health monitoring of complex structures if it is used as the sole temperature compensation technique.

5.3. *Combined use of the optimal baseline and the optimal stretch methods*

Figs. 11a and b show the results obtained when applying the optimal stretch method to compensate for a temperature difference between a current signal taken at 26.5 °C and reference signals taken 1 and 2 °C below that temperature, respectively, on the small plate. The worst value in the residual signal in Fig. 11a is above the 40 dB target value; however,

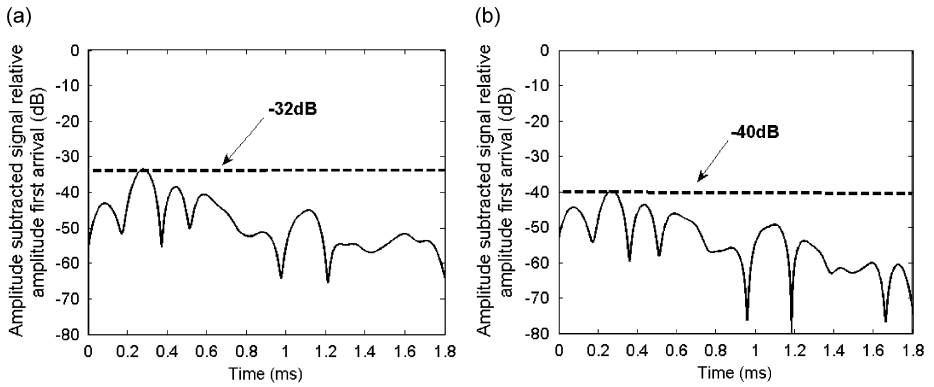

Fig. 11. (a) Amplitude of the subtracted signal relative to first arrival for (a) a 2 °C difference between current signal (26.5 °C) and reference (24.5 °C) after optimal stretch for small plate and (b) a 1 °C difference between current signal (26.5 °C) and reference (25.5 °C) after optimal stretch for small plate.

an improvement of −5 dB is seen compared to the level obtained in Fig. 10, when the temperature difference was 5 °C. When the temperature difference is further reduced, to 1 °C, the residual signal level is greatly improved, reaching the target value of −40 dB (Fig. 11b). This shows that although the optimal stretch method cannot be applied as the sole method for temperature compensation of complex structures, it can be used in conjunction with the optimal baseline method to reduce the number of baselines necessary to achieve target values of residual.

Therefore, if a number of baselines within the operating temperature range of a structure are collected, the following strategy can be applied: the optimal baseline method identifies the baseline providing the closest match to a signal taken during inspection and the optimal stretch method then compensates for remaining differences in temperature between the best baseline and the current signal. If such a strategy is applied to the small and large plates used in the experiments, the maximum gap between baselines to achieve the target levels of residual signal would be 1 °C for the small plate and 5 °C for the large plate. The increase in the maximum admissible temperature gaps between baselines makes collecting signals for the database an easier task since this gives a margin for temperature fluctuations in between data collections.

The maximum temperature difference that can be effectively compensated by the optimal stretch method is thought to decrease as more complex signals are processed. This suggests that the number of baselines needed for achievement of low levels of residue with such a processing strategy will increase with signal complexity. Nevertheless, the combination of the optimal baseline and the optimal stretch techniques will always require a smaller database than if the former is used alone.

The signal processing strategy consisting of the combination of the optimal stretch and the optimal baseline techniques will be used in the sections below.

5.4. Response to simulated defects

The response of the large and small plate systems to simulated defects was evaluated. As mentioned in Section 3, the simulated defect consisted of a brass cylinder with 5 mm diameter and 6 mm length attached to the surface of the plates with a couplant. The reflection ratio from this "defect" was estimated to be of the order of −24 dB, though it was strongly dependent on the coupling, making quantitative comparisons between the results in the two plates invalid. The reflection ratio was defined as the ratio of the amplitude of the reflection from the "defect" to the amplitude of the incident signal. This was measured by focusing a laser vibrometer at a point in-line between the transmitter and the "defect" at a position where the two signals could be separated in time. The amplitudes were corrected for propagation distances to correspond to the values at the "defect" location before computing the ratio.

A signal was taken at 26.5 °C on the two plates, with and without the "defect", and compared to a baseline 0.5 °C below this temperature, the "with defect" signals being taken the day after the baselines. The levels of the residual signal obtained by processing the signals acquired from the "undamaged" plate were compared to levels obtained from signals acquired with presence of the "defect".

Fig. 12a shows the time-trace obtained on the large plate with the "defect" and the residual signal left after processing and subtraction. In Fig. 12b the amplitude levels can be more easily identified and a first excursion above the "undamaged" residual values was seen at the time corresponding to the first arrival of a reflection from the "defect". This signal is 4 dB above the level of residual signal for the plate with no "defect", suggesting a reflection from the defect of less than −35 dB. This is much lower than the reflection ratio measured above due to the distance of the transducers from the defect. This illustrates that the detectability of a given defect is strongly dependent on the position relative to the transducers. The later parts of the signal are clearly disturbed and residual levels above −29 dB are found. This is caused by shadowing effects created by the presence of the "defect" which cause increases and decreases of amplitude in subsequent reflections from the edges of the plate.

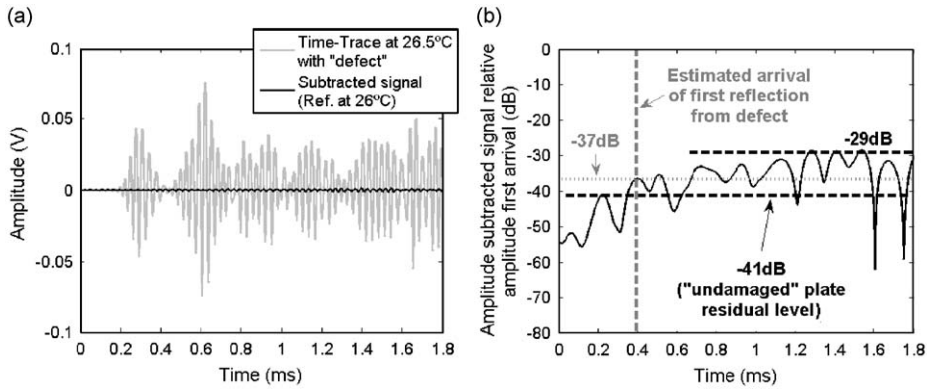

Fig. 12. (a) Signal taken at 26.5 °C on large plate with simulated defect and the signal obtained when subtracted from stretched reference (26 °C); (b) amplitude of the subtracted signal relative to amplitude of the first arrival in Fig. 12a.

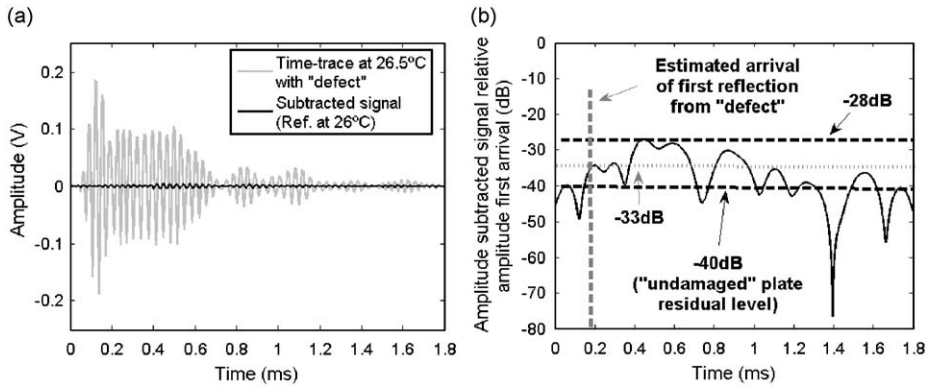

Fig. 13. (a) Signal taken at 26.5 °C on small plate with simulated defect and the signal obtained when subtracted from stretched reference (26 °C); (b) amplitude of the subtracted signal relative to amplitude of the first arrival in Fig. 13a.

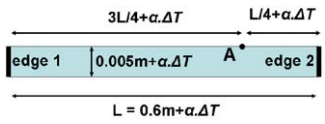

Fig. 14. Schematic diagram of geometry used for analytical simulation of signals with *A*0/*S*0 mode ratios similar to those obtained experimentally. As in Section 3, α is the coefficient of thermal expansion and ΔT is the change in temperature (in this case a 10 °C increase).

Fig. 13a shows the signal obtained from the small plate at 26.5 °C with the presence of a "defect" and the residual signal left after optimal stretch of the baseline and subtraction. Fig. 13b shows a first excursion 7 dB above the level for the "undamaged" plate. The presence of a defect in the small plate was relatively easy to detect compared to the large plate case. This is because the reduction of scale means the "defect" was closer to the transducers. However, as explained above, probable differences in the coupling of the simulated defects in the plates mean that precise quantitative comparisons should not be made. In Fig. 13b it can again be seen that the "defect" produces large changes in the later parts of the signal due to the shadowing effects discussed earlier.

6. Influence of mode purity on temperature compensation strategy

To evaluate the influence of mode purity on the signal processing strategy described in Section 5.3, signals were simulated analytically with the *A*0/*S*0 mode ratios which were obtained experimentally. The temperature variation was simulated by varying the dimensions of the plate and by changing the density, shear and longitudinal velocities of aluminium. These properties were obtained from data on the variation of elastic constants with temperature for monocrystalline aluminium found in Ref. [22]; this data was averaged according to Ref. [23] to give results for polycrystalline aluminium with crystals of cubic symmetry. This procedure was validated in Ref. [24] and used in Ref. [25]

giving good results. The property values derived from this procedure were used as input data to obtain frequency versus wavenumber curves at different temperatures from the software DISPERSE [26]. These curves were then used to simulate signals analytically as discussed, for example, in Ref. [27].

This 2D simulation was based on a 5 mm-thick, 0.6 m-long, aluminium plate shown in Fig. 14. The excitation was a five-cycle Hanning windowed toneburst centred in turn at each of the frequencies used experimentally. Propagation of the *A*0 and *S*0 modes in this plate at 20 and 30 °C was simulated. The signal was generated at edge 1 and then reflected backwards and forwards through the plate, being monitored at point A. In this case there is no mode conversion as the plate is mid-plane symmetric. For each reflection from the edges, the signal was phase shifted by 90° in the *A*0 mode case, while in the *S*0 mode case a 180° phase shift was applied [28]. The time-traces obtained for the *A*0 mode and the *S*0 mode were considered separately and were also added together to give signals with the *A*0/*S*0 mode ratios seen experimentally.

The time-traces in the pure mode and in the mixed mode states were processed with the Optimal Stretch method to compensate for the 10 °C difference between what was considered the reference signal (at 20 °C) and the current signal (at 30 °C). Fig. 15a shows the time-trace resulting from the simulation of the propagation of a five-cycle Hanning windowed toneburst centred at 200 kHz, with a *S*0/*A*0 mode ratio of 8 dB, in the geometry shown in Fig. 14. There is a clear *A*0 mode wave packet at around 0.25 ms, indicated by the second dark arrow from the left, which is roughly 2.5 times smaller than the amplitude of the *S*0 mode. The other *A*0 mode wave packets overlap with wave packets of the *S*0 mode as would happen with signals obtained experimentally. Fig. 15a also shows the signal resulting from the subtraction between the reference signal and the current signal after optimal stretch temperature compensation. Fig. 15b shows the amplitude of the subtracted signal relative to the first arrival in Fig. 15a. For comparison, the amplitude of the residual signal relative to the first arrival, when the same procedure is applied to the signal obtained with pure *S*0 is also shown.

Fig. 15b shows that the amplitude of the residual signal is increased in the regions where an *A*0 mode wave packet is present. This effect is most severe in later parts of the signal, reaching 15 dB at 1.7 ms, where the propagation distance for the *S*0 mode is about 9 m. For an *S*0 mode propagation distance of 5 m, which is reached at around 1 ms, the increase in amplitude levels in the residual signal was of the order of 10 dB.

The increased residual at the arrival time of *A*0 reflections indicates that the optimal stretch required for the *A*0 mode is different to that required for the *S*0 mode. Fig. 16 shows the variation of the rms value of the residual signal in the pure mode and mixed mode cases as a function of the percentage reduction of the frequency step size, Δf, in the spectrum, or the percentage stretch of the current signal. The minimum point in these curves corresponds to the optimal stretch. It is clear that the optimal stretch for pure *A*0 and pure S0 is different and that, as would be expected, the optimal stretch for an *S*0/*A*0 ratio of 8 dB is close to that for a pure *S*0 mode. However, the minimum value of the rms of the subtracted signal for the mixed mode case is slightly higher than for the pure S0 mode case; this is due to the localised increases in amplitude at times where the *A*0 mode wave packets were present.

The difference in the amount of stretch needed to achieve the minimum rms value of the subtracted signal for the *A*0 and the *S*0 modes during optimal stretch is a consequence of the effects described by Eq. (3), which shows that δt is proportional to v_{ph}^{-1} and γ. The large differences in phase velocity (v_{ph}) in the frequency-thickness product region used in this work are the dominant cause of the differences in stretch values between modes; the fractional change in phase velocity with temperature (γ) is also mode dependent but has less influence on the results presented here. The difference between the modes is amplified if the temperature difference between the signals being compared is large, since δt is directly proportional to δT. This means that the residual caused by differences in stretch values for mixed-mode signals will increase with the temperature difference between the reference and the current signals.

To evaluate experimentally the influence of mode purity on the temperature compensation techniques presented earlier, pairs of the two transducer types described in Section 3 were attached in turn to the 1m-square plate, at the positions shown in Fig. 1. The low-frequency *A*0 mode transducer was excited with a five-cycle toneburst centred at 35 kHz

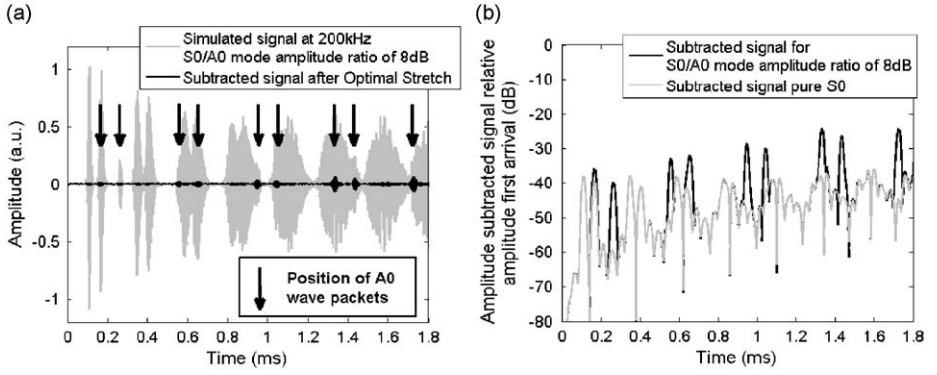

Fig. 15. (a) Simulated reference signal at 20 °C and subtracted signal after optimal stretch of simulated current signal at 30 °C, on structure shown in Fig. 14, with a 8 dB *A*0/*S*0 mode ratio; (b) amplitude subtracted signal relative to amplitude first arrival for pure *S*0 at 200 kHz and for signal with a 8 dB *A*0/*S*0 mode ratio.

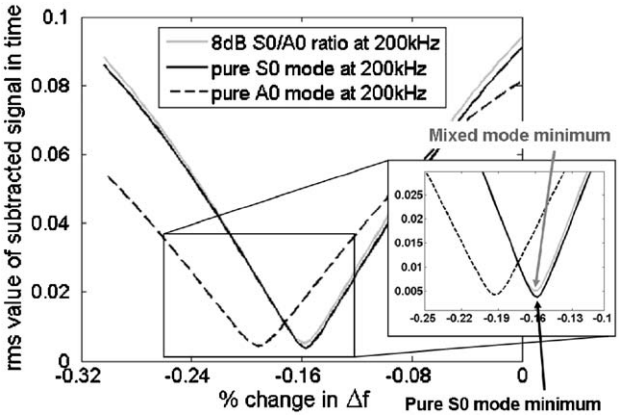

Fig. 16. Variation of position of minima in the rms value of the signal obtained from the subtraction between simulated reference signal at 20 °C and simulated current signal at 30 °C for pure *A*0 at 200 kHz, pure *S*0 at 200 kHz and a 8 dB *S*0/*A*0 mode ratio.

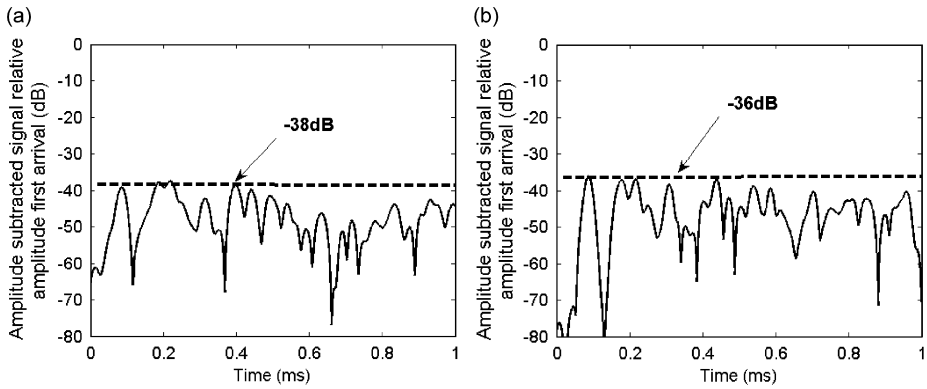

Fig. 17. Amplitude level in the residual signal relative to the first arrival, obtained after temperature compensation of a temperature gap of 0.5 °C between a reference and a current signal taken with (a) 17 dB *A*0/*S*0 mode ratio (150 kHz) and (b) 8 dB *S*0/*A*0 mode ratio (200 kHz). Structure: large plate.

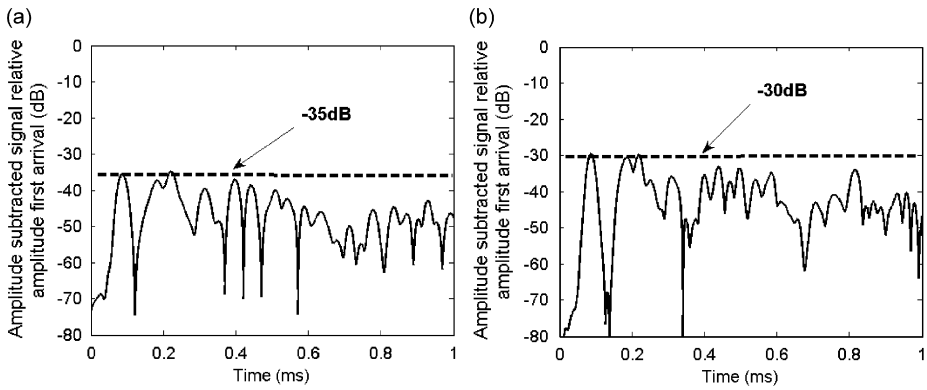

Fig. 18. Amplitude level in the residual signal relative to the first arrival, obtained after temperature compensation of a temperature gap of 2 °C between a reference and a current signal taken with (a) 17 dB *A*0/*S*0 mode ratio (150 kHz) and (b) 8 dB S0/*A*0 mode ratio (200 kHz). Structure: large plate.

and this gave a *A*0/*S*0 mode ratio of 73 dB in pitch-catch. The piezoelectric disc was excited with a five-cycle toneburst centred at 150 and 200 kHz, giving 17 and 8 dB *S*0/*A*0 mode ratios, respectively.

Fig. 17a shows the results obtained using optimal stretch with a temperature difference of 0.5 °C between the reference and the current signal taken from the system operating with the piezoelectric disc transducer at 150 kHz. The amplitude levels in the subtracted signal after optimal stretch achieved values close to the target levels (−38 dB relative to the first arrival). Fig. 17b shows the results with the same temperature difference between reference and current signal, for the

same system at 200 kHz. In this case the worst case amplitude level resulting from the subtraction of the two signals after optimal stretch is −36 dB.

Fig. 18 shows the corresponding results with a temperature difference of 2 °C between the reference signal and the current signal. The increase in the temperature gap between the two signals leads to an increase in residual levels to −35 dB at 150 kHz and −30 dB at 200 kHz. The results in Figs. 17 and 18 are shown up to a time corresponding to a propagation of around 5 m of the *S*0 mode.

When the signals obtained with the low-frequency *A*0 mode transducer pair were processed with 0.5 °C and a 2 °C temperature gaps between baseline and current signals, the worst residual signal level obtained after subtraction was −40 and −39 dB, respectively. This was expected since it was shown previously (Fig. 9) that in this case a temperature gap of 5 °C can be satisfactorily compensated for using optimal stretch.

The results in Figs. 17 and 18 show that if the temperature difference between the baseline and the current signals is small, good levels of residual signal are obtained after subtraction by using the signal processing strategy described in Section 5.3. However, if the temperature difference increases, the difference in the stretch factor required for the two modes becomes significant and the degree of mode purity becomes an important factor in the quality of the result obtained.

It is important to stress that mode purity is not the only factor in the difference between the residual of Figs. 18a and b. Eq. (7) shows that the residual is proportional to the number of wavelengths propagated. A 5 m propagation distance is equivalent to 138 *S*0 mode wavelengths at 150 kHz and 185 wavelengths at 200 kHz. Therefore, a difference of 2.5 dB in the residuals at the two frequencies due to this effect would be expected. This suggests that the increase of 5 dB between Fig. 18a and b is half due to the effects of mode purity and half to the increase in number of wavelengths propagated.

7. Inspection of a real structure

As an example of inspection of a real structure, a section of an airframe panel, shown in Fig. 19, was used. The main structural features in this were steps in thickness (from 2 to 1 mm) and bonded stiffeners, as well as the edges. This panel was instrumented with three low-frequency *A*0 mode transducers, one of them being used as an emitter and the other two as receivers. The system was placed in a room with no temperature control where temperature variations of up to 4–5 °C were common. The acquisition system consisted essentially of the same equipment used for previous experiments, the only difference being the use of a multiplexer to switch between receiving channels. Signals were acquired every 2 h over 3 weeks and this supplied a set of baselines in which temperature gaps between signals never exceeded 0.3 °C.

It is known that large temperature gradients within the structure can limit the applicability of this temperature compensation strategy since this would invalidate the baselines collected previously. In this specific test, only small temperature gradients, below 1 °C, were encountered; work in progress [29] suggests, however, that temperature gradients of up to 2 °C in large metallic structures can be accommodated by the compensation strategy.

The features in the propagation path between the emitter and the first receiver were a 50 percent reduction in thickness, from 2 to 1 mm, and a stiffener, while an additional two stiffeners and an increase in thickness back to that at the emitter were present in between the two receivers. The distance from the emitter to point A in Fig. 19b and back to each of the receivers was considered the propagation distance needed to ensure complete coverage. This distance was 1.58 m for receiver 1 and 1.28 m for receiver 2.

The signals obtained on this structure were processed with the optimal baseline Subtraction method alone and with the combined optimal baseline subtraction and the optimal stretch techniques. Fig. 20a shows the time-trace obtained at

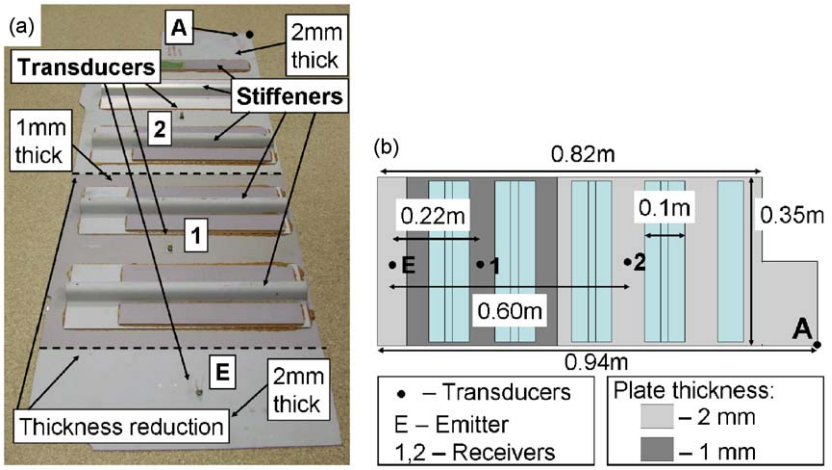

Fig. 19. Airframe panel used for inspection of a real structure-like specimen. (a) Picture; (b) schematic diagram with distances.

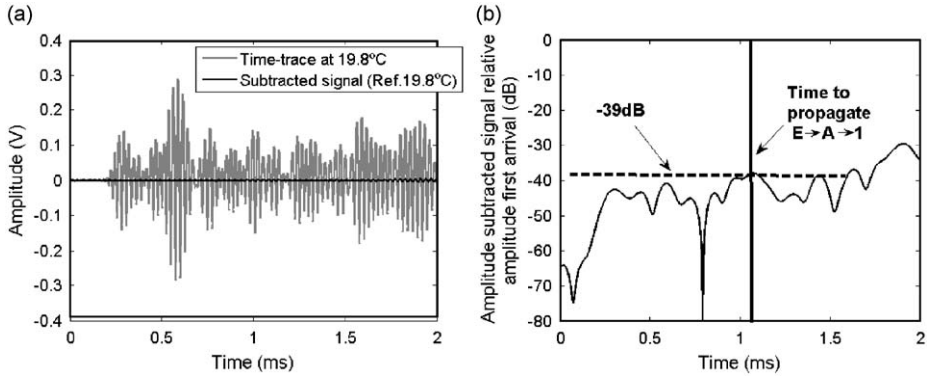

Fig. 20. (a) Signal taken at 19.8 °C at receiver 1 on airframe panel and the residual signal obtained when subtracted from optimal baseline (19.8 °C); (b) amplitude of the subtracted signal relative to amplitude of the first arrival in Fig. 20a.

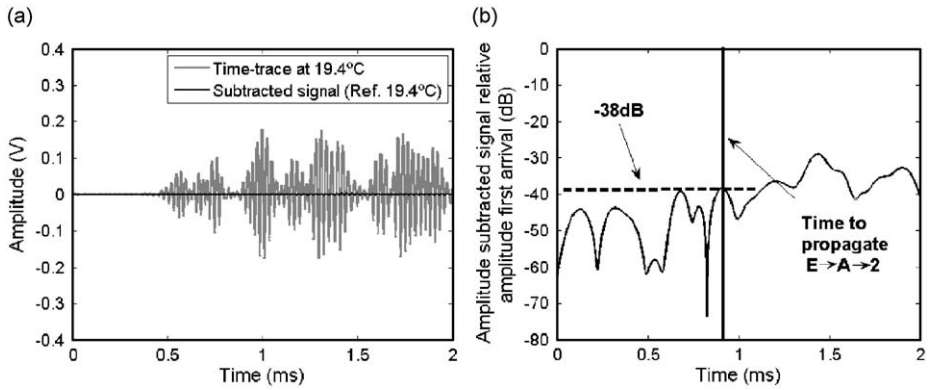

Fig. 21. (a) Signal taken at 19.8 °C at receiver 2 on airframe panel and the residual signal obtained when subtracted from optimal baseline (19.8 °C); (b) amplitude of the subtracted signal relative to amplitude of the first arrival in Fig. 21a.

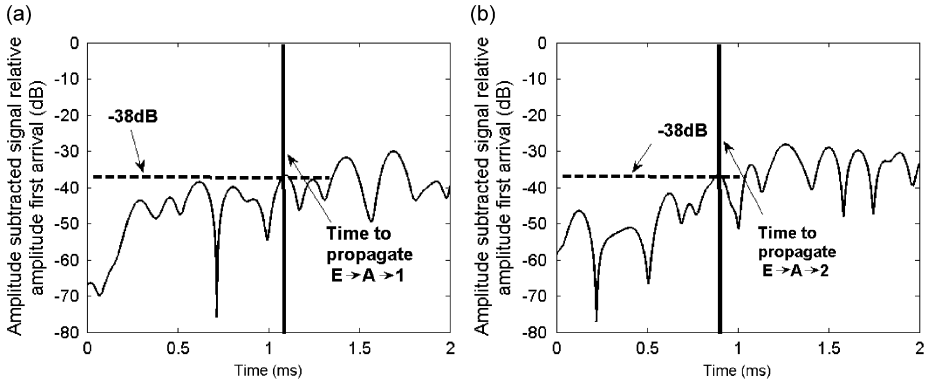

Fig. 22. Amplitude level in the residual signal relative to the first arrival, obtained after temperature compensation of a temperature gap of 0.5 °C between a reference and a current signal taken at: (a) receiver 1; (b) receiver 2.

receiver 1 (see Fig. 19b). Signals are shown up to a time equivalent to a propagation distance of 3 m for the *A*0 mode at 35 kHz. In Fig. 20a, the residual signal obtained after direct subtraction of the optimal baseline, which was a signal taken at the same temperature in the previous week, is also shown. The level of the residual signal relative to the amplitude of the first arrival in Fig. 20a is shown in Fig. 20b. It can be seen that a residual level of −39 dB is achieved up to times considerably above that needed for full coverage of the structure.

Fig. 21a shows the signal received at receiver 2 on the airframe panel and the subtracted signal obtained after direct subtraction from the optimal baseline which was also taken at the same temperature in the previous week. Fig. 21b shows that in this case residual signal amplitude levels of −38 dB relative to the first arrival in Fig. 21a are also obtained up to the time necessary for full coverage of the panel.

Figs. 22a and b show the result of processing signals obtained at receivers 1 and 2, respectively, when the signal processing strategy, consisting of the combination of the optimal baseline subtraction method and the optimal stretch method, was applied to signals obtained from the structure at 21.4 and 21.9 °C, giving a difference of 0.5 °C. Residual amplitude levels of −38 dB are achieved up to times significantly above the time which is necessary for full coverage in both cases. These results show that this temperature compensation strategy is efficient in delivering residual levels as low as those found when the optimal baseline subtraction technique is used alone, even though a smaller number of baselines in the database were used. If a 1 °C temperature gap between baseline and current signal was used, the maximum amplitude level in the residual signal up to the time equivalent to full coverage increased to around −34 dB relative to the first arrival. Therefore, in this case the complexity of the signals means that baselines must be acquired with a maximum temperature gap of around 0.5 °C.

8. Conclusions

When the optimal baseline subtraction method is used alone as a temperature compensation technique, a large number of baselines are needed since only small temperature steps (typically 0.1 °C) will ensure amplitude levels in the residual signal which are low enough for good sensitivity (around −40 dB relative to the first arrival). The success of the optimal stretch method is strongly dependent on mode purity and structural complexity. However, if signal complexity is low and mode purity is high, it is effective in compensating for a large temperature gap between reference and current signals (>5 °C).

The optimal baseline subtraction and the optimal stretch methods can be combined to form a robust temperature compensation strategy. This reduces the number of baselines necessary to ensure good sensitivity in comparison to that needed when the optimal baseline subtraction technique is used alone. The reduction in the number of baselines in the database is limited by the maximum temperature gap between baselines which can be compensated for by the optimal stretch without loss of sensitivity; this is a function of mode purity, signal complexity and the maximum propagation distance to cover the whole structure expressed in wavelengths. In some cases, especially when the signal complexity is high or when mode purity is insufficient, the temperature gap between baselines needed for good sensitivity can drop to as low as 0.5 °C, as was seen for the airframe structure inspected. In this case, the signal processing strategy gave a residual of −38 dB with a temperature gap of 0.5 °C, when high mode purity was used. If the temperature gap was increased to 1 °C the residual amplitude was worsened, to −34 dB.

When this signal processing strategy was used to process signals obtained from undamaged plates and from the same plates with simulated damage, a first excursion above the residual level for the undamaged structure was seen in the expected position of the first reflection from the "defect". Large increases in later parts of the residual signals were also seen, indicating good sensitivity to changes in the structure.

Acknowledgements

The authors would like to thank EPRSC for funding of the project. T. Clarke would like to thank the CAPES agency of the Brazilian Government for personal funding in the form of a PhD scholarship.

References

[1] T.E. Michaels, J.E. Michaels, Sparse ultrasonic transducer array for structural health monitoring, in: D.O. Thompson, D.E. Chimenti (Eds.), *Review of Progress in Quantitative Nondestructive Evaluation*, Vol. 23, American Institute of Physics, New York, 2004, pp. 1468–1475.
[2] X. Zhao, H. Gao, G. Zhang, B. Ayhan, F. Yan, C. Kwan, J.L. Rose, Active health monitoring of an aircraft wing with embedded piezoelectric sensor/actuator network: I. Defect detection, localization and growth monitoring, *Smart Materials and Structures* 16 (2007) 1208–1217.
[3] B. Xu, V. Giurgiutiu, Single mode tuning effects on Lamb wave time reversal with piezoelectric wafer active sensors for structural health monitoring, *Journal of Nondestructive Evaluation* 26 (2007) 123–134.
[4] J.-B. Ihn, F.-K. Chang, Pitch-catch active sensing methods in structural health monitoring, *Structural Health Monitoring* 7 (1) (2008) 5–19.
[5] M. Lemistre, D. Balageas, Structural health monitoring system based on diffracted Lamb wave analysis by multiresolution processing, *Smart Materials and Structures* 10 (2001) 504–511.
[6] S. Grondel, J. Assad, C. Delabarre, E. Moulin, Health monitoring of a composite wingbox structure, *Ultrasonics* 42 (2004) 819–824.
[7] H.W. Park, H. Sohn. K.H. Law, C.R. Farrar, Time reversal active sensing for health monitoring of a composite plate, *Journal of Sound and Vibration* 302 (2007) 50–66.
[8] K. Worden, C.R. Farrar, G. Manson, G. Park, The fundamental axioms of structural health monitoring, *Proceedings of the Royal Society A* 463 (2007) 1639–1664.
[9] J.E. Michaels, T.E. Michaels, Detection of structural damage from the local temporal coherence of diffuse ultrasonic signals, *IEEE Transactions on Ultrasonics, Ferroelectrics, and Frequency Control* 52 (10) (2005) 1769–1782.
[10] M.J.S. Lowe, P. Cawley, J.-Y. Kao, O. Diligent, The low frequency reflection characteristics of the fundamental antisymmetric Lamb wave a0 from a rectangular notch in a plate, *Journal of the Acoustical Society of America* 112 (2002) 2612–2622.
[11] O. Diligent, T. Grahn, A. Bostrom, P. Cawley, M.J.S. Lowe, The low frequency reflection and scattering of the S0 Lamb mode from a circular through thickness hole in a plate: finite element, analytical and experimental studies, *Journal of the Acoustical Society of America* 112 (2002) 2589–2601.
[12] O. Diligent, M.J.S. Lowe, P. Cawley, P. Wilcox, Reflection of the S0 Lamb mode from a part-depth circular defect in a plate when the incident wave is created by a small source, in: D.O. Thompson, D.E. Chimenti (Eds.), *Review of Progress in Quantitative Nondestructive Evaluation*, Vol. 22, American Institute of Physics, 2003, pp. 197–204.

[13] A. Demma, P. Cawley, M.J.S. Lowe, Scattering of the fundamental shear horizontal mode from steps and notches in plates, *Journal of the Acoustical Society of America* 113 (2003) 1880–1891.
[14] R.L. Weaver, O.I. Lobkis, Temperature dependence of diffuse field phase, *Ultrasonics* 38 (2000) 491–494.
[15] Y. Lu, J.E. Michaels, A methodology for structural health monitoring with diffuse ultrasonic waves in the presence of temperature variations, *Ultrasonics* 43 (2005) 717–731.
[16] A.J. Croxford, P.D. Wilcox, B.W. Drinkwater, G. Konstantinidis, Strategies for guided wave structural health monitoring, *Proceedings of the Royal Society A* 463 (2007) 2961–2981.
[17] A.J. Croxford, P. D. Wilcox, G. Konstantinidis, B.W. Drinkwater, Strategies for overcoming the effect of temperature on guided wave structural health monitoring, T. Kundu (Ed.), *Proceedings of SPIE*, Vol. 6532, 2007, pp. 65321T-1–65321T-10.
[18] R. Ramesham, R. Ghaffarian, Challenges in interconnection and packaging of micromechanical systems (MEMS), *Proceedings of the 50th Electronic Components and Technology Conference*, IEEE, New Jersey, 2000, pp. 666–675.
[19] ABAQUS User's Manual, version 6.7-1, 2008.
[20] T. Clarke, F. Simonetti, S. Rokhlin, P. Cawley, Evaluation of the temperature stability of a low-frequency *A*0 mode transducer developed for SHM applications, D.O. Thompson, D.E. Chimenti (Eds.), *Review of Progress in Quantitative Nondestructive Evaluation*, vol. 27, 2008, pp. 910–917.
[21] O.I. Lobkis, R.L. Weaver, Coda-wave interferometry in finite solids: recovery of P-to-S conversions rates in an elastodynamic billiard, *Physical Review Letters* 90 (2003) 254302-1–254302-4.
[22] P.M. Sutton, The variation of the elastic constants of crystalline aluminium with temperature between 63 K and 773 K, *Physical Review* 91 (1953) 816–821.
[23] R.W. Hill, The elastic behaviour of a crystalline aggregate, *Proceedings of the Physical Society of London A* 65 (1952) 349–354.
[24] O.L. Anderson, in: W.P. Mason (Ed.), *Physical Acoustics*, Vol. IIIB, Academic Press, New York, 1965.
[25] S.I. Rohklin, An ultrasonic bridge for the study of viscoelastic properties of thin interface films, *Journal of the Acoustical Society of America* 73 (1983) 1619–1623.
[26] M.J.S. Lowe, Matrix techniques for modeling ultrasonic waves in multilayered media, *IEEE Transactions on Ultrasonics, Ferroelectrics, and Frequency Control* 42 (4) (1995) 525–542.
[27] P.D. Wilcox, M.J.S. Lowe, P. Cawley, A signal processing technique to remove the effect of dispersion from guided wave signals, in: D.O. Thompson, D.E. Chimenti (Eds.), *Review of Progress in Quantitative Nondestructive Evaluation*, Vol. 20, American Institute of Physics, New York, 2001, pp. 555–562.
[28] P. Torvik, Reflection and wave trains in semi-infinite plates, *Journal of the Acoustical Society of America* 41 (1967) 346–353.
[29] T. Clarke, P. Cawley, Evaluation of the damage detection capability of a sparse-array guided wave SHM system applied to a real structure, in preparation.